Applied Surface Science 508 (2020) 145233

Contents lists available at ScienceDirect

Applied Surface Science

journal homepage: www.elsevier.com/locate/apsusc

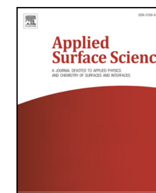

Full Length Article

Tunable structure and connectivity of organosilica hybrid films by using different epoxy based precursors in atmospheric plasma deposition

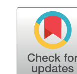

R. Moriche[a,b,*], Y. Ding[c], S. Dong[c], O. Zhao[c], R.H. Dauskardt[c,*]

[a] Materials Science and Engineering Area, University Rey Juan Carlos, C/Tulipán s/n, Móstoles, 28933 Madrid, Spain
[b] Dpto. de Física de la Materia Condensada, ICMS, CSIC-Universidad de Sevilla, Apdo. 1065, 41080 Sevilla, Spain
[c] Department of Materials Science and Engineering, Stanford University, Stanford, CA 94305-2205, USA

ARTICLE INFO

Keywords:
Hybrid film
Organosilica
Fluorinated
Atmospheric plasma deposition

ABSTRACT

Organosilica hybrid films and fluorinated organosilica hybrid films have been successfully deposited using atmospheric plasma deposition. Different precursors, which incorporates epoxy groups in their molecules, were used to obtain connected structures with tunable chemistry and connectivity. The study demonstrated the capability of tuning the chemical composition, connectivity and mechanical properties of organosilica films by selecting the precursors and operational parameters of the process. The use of (3-glycidiloxypropyl) trimethoxysilane (GPTMS) and 2-(3,4-epoxy-cyclohexylethyl) trimethoxysilane (TRIMO) as precursors made possible the deposition of hybrid films with high organic character, increasing the relative C content up to 20 at% and 40 at%, respectively, due to the lower fragmentation caused during the deposition by atmospheric plasma. The obtained structures had higher concentration of symmetric cages than those obtained from precursors without epoxy groups, which lead to a more compact structure and higher stiffness than conventional organic films. The combination with a fluorinated molecule also had a strong influence in the resultant structure caused by the preferential orientation of fluorinated molecules due to the low surface energy of FDTS that causes migration of fluorinated tails to the film-air interface during the film growth.

1. Introduction

During the last decade, organo-inorganic molecular hybrid materials has become of interest in many fields due to their properties between inorganic and organic materials [1]. Unlike conventional nanocomposites which are made of physical mixture of separated phases, the intimate mixing of the organic and inorganic components in molecular hybrids at the molecular scale leads to unique properties and functionalities that is not simply a sum of the individual components [2]. Particularly, the advantages of organosilica, in comparison with the inorganic SiO_2, are their light-weights, [3] better adhesive properties to the organic substrates due to the increasing coating plasticity [4], better moisture resistance [5], and so on.

In general, silane precursors containing organic functional groups are used to synthesis the organo-inorganic molecular hybrids. One of the advantages of these hybrid films is that these precursors can react with a wide range of substrates, both organic and inorganic. Additionally, some organic functional groups such as epoxy ring or vinyl groups can undergo in-situ polymerization reaction to form a connected organic networks [4], which is possible to increase the fracture toughness and moisture resistance of the coatings [5].

Traditionally, these coatings have been deposited using the sol-gel method. However, the coating connectivity is usually low if high processing temperature is prohibited [6]. Although there are many publications using conventional vacuum plasma technologies for making high quality films with enhanced network connectivity [7,8], the use of atmospheric plasma deposition to grow functional coatings has an increasing interest [9]. The main advantages of this technology is the reduction of costs and the higher production throughput [10] due to the absence of vacuum.

Although post discharge atmospheric plasma has lower deposition rates, depending on different parameters such as distance between the substrate and the plasma source and precursors flow, there is a lower fragmentation of the mentioned precursors as well as the lower damage induce to the substrate [11]. This lower fragmentation leads to different reaction mechanisms during the growth of the films, which can result in different chemical compositions and connectivity [12] but also to controlled deposition rate and properties.

* Corresponding authors at: Dpto. de Física de la Materia Condensada, ICMS, CSIC-Universidad de Sevilla, Apdo. 1065, 41080 Sevilla, Spain (R. Moriche) and Department of Materials Science and Engineering, Stanford University, Stanford, CA 94305-2205, USA (R. H. Dauskardt).
E-mail addresses: rmoriche@us.es (R. Moriche), dauskardt@stanford.edu (R.H. Dauskardt).

https://doi.org/10.1016/j.apsusc.2019.145233
Received 8 April 2019; Received in revised form 21 November 2019; Accepted 30 December 2019
Available online 02 January 2020
0169-4332/ © 2020 Elsevier B.V. All rights reserved.

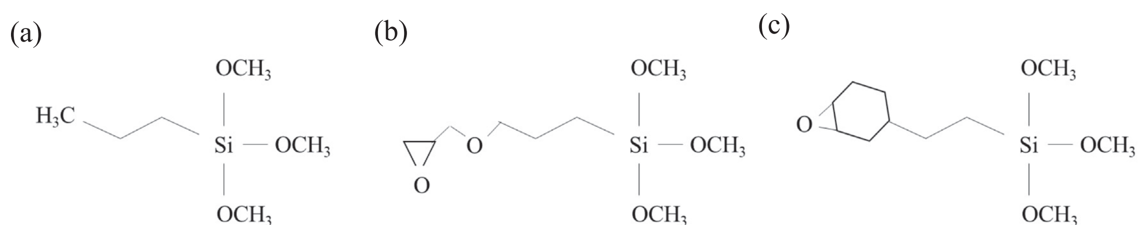

Fig. 1. Precursors for organosilica film atmospheric plasma deposition: (a) trimethoxy(propyl) silane (ETHER), (b) (3-glycidiloxypropyl) trimethoxysilane (GPTMS) and (c) 2-(3,4-epoxy-cyclohexylethyl) trimethoxysilane (TRIMO).

In this study, we analyze how chemical composition, molecular structure and connectivity of hybrid organosilica films deposited by atmospheric plasma deposition can be controlled and tuned by the selection of different precursors and plasma operative conditions in order to have customized properties. Three different organic precursors are used for deposition: trimethoxy(propyl) silane (ETHER), (3-glycidiloxypropyl) trimethoxysilane (GPTMS) and 2-(3,4-epoxy-cyclohexylethyl) trimethoxysilane (TRIMO), whose molecules are shown in Fig. 1. The aim of using these precursors is the analysis of the influence of epoxide and cyclohexyl groups into the molecule in deposition and structure of the hybrid films. Compared to ETHER, both GPTMS and TRIMO have epoxides which can potentially open and polymerize to form a connected organic network with plasma activations. Moreover, the ring tension caused by the cyclohexyl group structure present in TRIMO significantly increases the epoxy ring activity and may increase the organic network connectivity in the hybrid molecular structure. The dependence of the films stiffness on the chemical composition and connectivity was also studied. Additionally, the process was optimized for the incorporation of fluorinated molecules into the structure of the organosilica hybrid films. For this purpose, 1H, 1H, 2H, 2H-perfluorodecyltriethoxysilane (FDTS) was simultaneously used as precursor. The influence in chemical composition and connectivity, as well as in efficiency of the atmospheric plasma deposition, of the incorporation of FDTS as secondary precursor was analyzed.

2. Experimental methods

2.1. Films atmospheric deposition

Organosilica films were deposited using an atmospheric 300 W RF plasma source (*Atomflow A500, Surfx Technologies LLC,* US). The scanning of substrates was carried out by a linear plasma head and a scanning stage.

Trimethoxy(propyl) silane (ETHER, > 98%, *Sigma Aldrich*) was used as precursor to grow organosilica films. The evaporation was carried out at 30 °C and the deposition parameters for this precursor are detailed in Table 1.

Two different precursors with epoxy groups were used, (3-glycidiloxypropyl) trimethoxysilane (GPTMS, > 98%, *Sigma Aldrich*) and 2-(3,4-epoxy-cyclohexylethyl) trimethoxysilane (TRIMO, > 97%, *Sigma Aldrich*). Plasma was created with 20 L/min of Ar, as the primary gas, and O_2, whose flow rate was dependent on the plasma power used during operation. The precursors were heated up to 120 °C and then delivered directly after the plasma glow region using a flow rate of 0.3 L/min and a dilution rate of 2 L/min with high purity Ar. The deposition parameters used in each case are detailed in Table 2.

Table 1
Deposition parameter used in organosilica coatings obtained from ETHER.

Precursor		ETHER			
		E60	E80	E100	E120
Parameter	Unit				
Primary plasma gas (flow rate)	L/min	20.0	20.0	20.0	20.0
Secondary plasma gas (flow rate)	L/min	0.08	0.08	0.10	0.15
Plasma power	W	60	80	100	120
Bubbler gas flow rate	L/min	0.15	0.15	0.15	0.15
Dilution gas flow rate	L/min	2.00	2.00	2.00	2.00
Deposition distance	mm	7	7	7	7
Linear plasma head speed	mm/s	25	25	25	25
Step	mm	1	1	1	1

In order to achieve fluorinated organosilica films, 1H, 1H, 2H, 2H-perfluorodecyltriethoxysilane (FDTS, > 97%, *Sigma Aldrich*) was used as additional precursor. This precursor was delivered and mixed with the epoxy-based ones, i.e. GPTMS and TRIMO to obtain the G/F and T/F films, respectively. The evaporation of FDTS was carried out at room temperature, which was set from calculations of the evaporation rates for the given gas flow and limits to form good quality coatings, and the deposition parameters used were the same of G100 and T100, whose deposition parameters are detailed in Table 2, but with optimized bubbler (main precursor for network formation) and dilution gas (FDTS) flows as indicated in Table 2.

Coatings were deposited on standard silicon wafer with $20 \times 15 \times 0.78\ mm^3$. Silicon substrates were cleaned with isopropanol and UV-Ozone for 5 min (*UVO-Cleaner 144 AX, Jelight Company, Inc.*, USA) prior to deposition.

2.2. Structural characterization

The thickness of deposited films was measured using a surface profilometer (*Veeco Dektak 150, Veeco Instrument Inc.*, USA).

Atomic contents of Si, C and O of as-prepared coatings were measured by X-ray photoelectron spectroscopy (XPS, *PHI 5000 Versaprobe, Physical Electronics Inc.*, USA). An Al-Kα X-ray source (1486 eV) with a spot size of 1 mm was used in a scanning range from 0 to 1000 eV (1 eV/step). Before each measurement, surfaces were ion sputtered for 0.5 min (~5nm) in order to remove any surface contaminants.

Fourier-transform Infrared spectroscopy (FTIR) was used to study chemical bonds in coatings utilizing a *Nicolet iS50 FT/IR Spectrometer* (*ThermoFisher Scientific Inc.*, USA). The FTIR spectra were recorded from 650 to 4000 cm^{-1} with a resolution of 4 cm^{-1}.

Additionally, Atomic Force Microscopy (AFM) was carried out in a *Bruker BioScope Resolve BioAFM* (*Bruker*, USA) in order to evaluate the surface quality and roughness of the deposited films.

2.3. Mechanical and adhesion properties

Nanoindentation tests were performed to characterize the Young's modulus of the coatings deposited on silicon wafers. The tests were carried out in dynamic mode with a load up to 50 mN and diamond Berkovich probe in a *iNano* nanointation equipment from *Nanomechanics Inc*. The Young's modulus of the films were calibrated using the Oliver Pharr method [13].

Table 2
Deposition parameter used in organosilica coatings obtained from precursors with epoxy groups: GPTMS and TRIMO.

Precursor		GPTMS					TRIMO				
		G60	G80	G100	G120	G/F	T60	T80	T100	T120	T/F
Parameter	Unit										
Primary plasma gas (flow rate)	L/min	20.0	20.0	20.0	20.0	20.0	20.0	20.0	20.0	20.0	20.0
Secondary plasma gas (flow rate)	L/min	0.08	0.08	0.10	0.15	0.10	0.08	0.08	0.10	0.15	0.10
Plasma power	W	60	80	100	120	120	60	80	100	120	100
Bubbler gas flow rate	L/min	0.30	0.30	0.30	0.30	0.20	0.30	0.30	0.30	0.30	0.18
Dilution gas flow rate	L/min	2.00	2.00	2.00	2.00	0.10	2.00	2.00	2.00	2.00	0.12
Deposition distance	mm	7	7	7	7	7	7	7	7	7	7
Linear plasma head speed	mm/s	25	25	25	25	25	25	25	25	25	25
Step	mm	1	1	1	1	1	1	1	1	1	1

3. Results and discussion

3.1. Chemical composition and connectivity of organosilica films

3.1.1. Chemical composition

As mentioned above, it has been demonstrated by several authors that the adhesive properties of organosilica films increases with the organic content due to the increment of overall coating plasticity contribution to the coating adhesion energy [14]. In order to elucidate how the selection of a proper precursor can strongly condition the chemical composition of hybrid films, the atomic percentages of Si, O and C of the deposited coatings, calculated from the full XPS spectra, are shown in Fig. 2. It can be seen that using ETHER (E-films) as precursor, resultant films have Si contents around 30 at% (Fig. 2a), O contents around 70 at% (Fig. 2b) and negligible C contents (Fig. 2c). These values are nearly independent on the power used during deposition. It is also important to notice, that the O/Si ratio in these coatings is ~2 (Fig. 3), which is the ratio of the inorganic SiO_2 structure, revealing the inorganic character of the coatings with a dominant SiO_2-like structure.

In contrast, if GPTMS (G-films) and TRIMO (T-films) are used as precursors, the relative amount of Si atoms decreases (Fig. 2a) and the C content significantly increases in both cases (Fig. 2c), achieving values of ~20% and ~40%, respectively, when the deposition is carried out with a plasma power of 60 W. When the power used during deposition increases, the C/Si ratio of the films strongly diminishes leading to a major relative concentration of Si and O atoms in the created network (Fig. 3). This fact makes atomic contents more similar to the ones of the E-films as the plasma power is higher. Therefore, by increasing the power, the inorganic character of the coatings increases, obtaining a structure closer to the one of SiO_2. This phenomenon was observed previously when dipodal silanes were used as the precursors and was explained by the precursor fragmentation and oxidation under harsh plasma conditions [15].

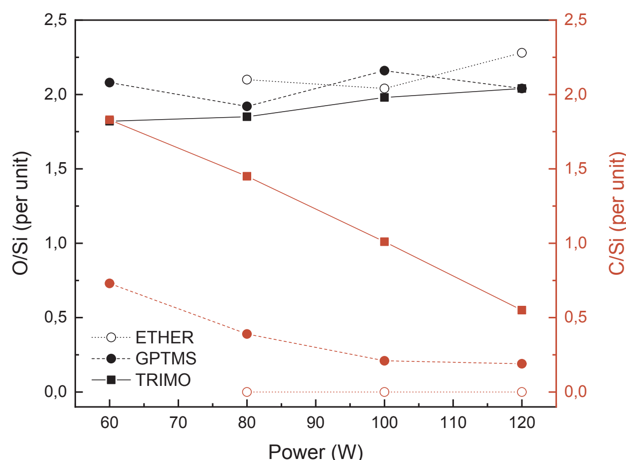

Fig. 3. O/Si and C/Si ratios of deposited coatings using ETHER, GPTMS and TRIMO as precursors.

Nevertheless, although tendencies are similar, the use of TRIMO as precursor, related to GPTMS, in atmospheric plasma deposition increases the C content of the organosilica coatings near 100% considering coatings deposited with the same power. As it has been explained, the main reasons are the different C contents initially into the precursors molecules and the lower tendency to fragmentation of the different precursors, already mentioned, as the cyclohexyl group needs two cleavages of C-C bonds, which leads to differences in plasma chemistry and, therefore, in films composition.

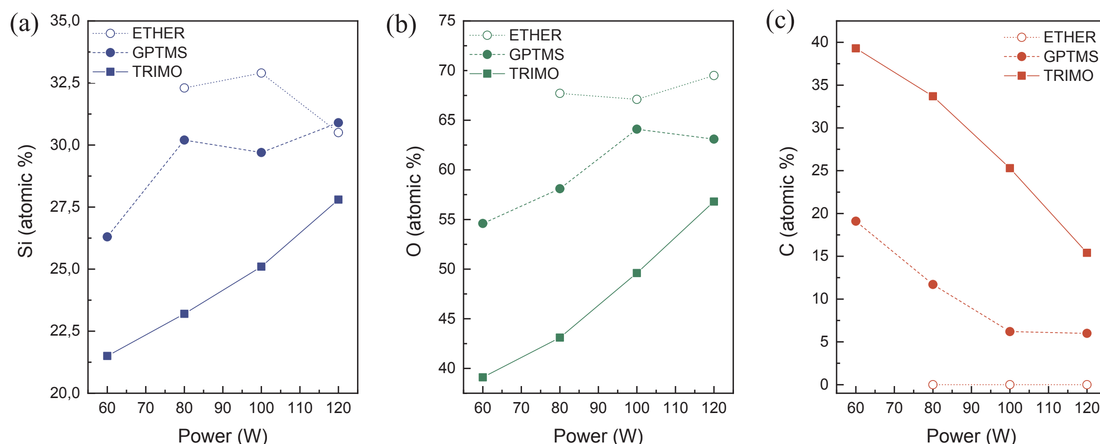

Fig. 2. Chemical composition of different coatings using ETHER, GPTMS and TRIMO as precursors: (a) Si, (b) O and (c) C atomic contents.

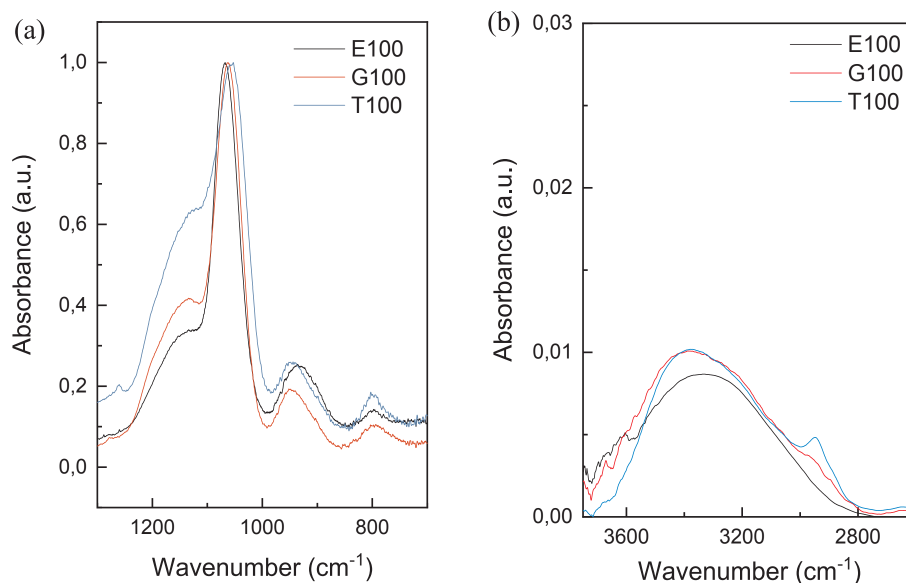

Fig. 4. FTIR spectra of deposited coating using ETHER, GPTMS and TRIMO as precursors with a plasma power of 100 W: (a) 700–1300 cm^{-1} and (b) 2700–3700 cm^{-1}.

3.1.2. Influence of the precursor molecule in connectivity of organosilica films

In order to analyze the chemical structure and connectivity of deposited films, FTIR vibrational modes were studied. Fig. 4 shows the FTIR spectra of the deposited coatings for each precursor as a function of the plasma power used during deposition.

Fig. 4a shows the spectra of the E100, G100 and T100 coatings. The asymmetric stretching of Si—O—Si can be clearly observed in all cases, which has been previously reported to appear in the range between 1075 and 1108 cm^{-1}. This peak is the result of three contributions due to different connectivity between Si and O atoms. Peaks at 1129, 1063 and 1023 cm^{-1} are associated to Si—O—Si cage like structure, Si—O—Si network and Si—O—Si sub-oxide structure, respectively [16,17]. Therefore, the connectivity of G100 and T100 films has a higher contribution of organic networks as the peak shifts to lower values of wavelengths. The shift to wavelengths lower than 1063 cm^{-1} in the case of G100 and T100, in some reported cases down to 1050 cm^{-1}, is attributed to longer Si—O—Si chains but can also be due to the appearance of open cages [15]. In both of the cases, it implies a less symmetric and more random structure with more fraction of open cages. When highly symmetric cages are formed in the organosilica structure, a vibrational mode at 1140 cm^{-1} can be observed. This peak can be also observed in E100, G100 and T100 but with a higher contribution in G100 and even higher in T100. This fact also supports evident differences in the connectivity of the structure, as using precursors with epoxy groups promotes formation of more symmetric cages and a more compact structure [18]. Additionally, the higher intensity of the peak located at ~1075 cm^{-1}, resultant from Si—O—Si contributions, in E and G films is an indicator of the formation of new Si—O—Si bonds [19]. It is important to note that the epoxide ring deformation band at 1257 cm^{-1} and the antisymmetric epoxide ring deformation bands at 755 and 907 cm^{-1} [20] were not observed in G and T films after deposition, indicating that all the epoxy groups have reacted, which indicates the formation a connected organic network. It is important to note that the opening of the epoxy ring occurs at relative high temperatures or at low temperatures with the use of catalysts in sol-gel processes, so atmospheric plasma makes possible to promote this opening to achieve the connected organic network already mentioned.

The broad band at 3450 cm^{-1}, which can be observed in Fig. 4b, is associated to OH stretching vibration of Si—OH and the peak at 2950 cm^{-1} corresponds to the CH_3 and CH_2 stretch region [21]. This peak is stronger in T films, has lower intensity in G films and is absent E films, so the incorporation into the precursor molecule of the cyclohexyl and epoxy groups leads to a higher chemical stability of the molecule, which results in a higher C content as indicated above [22].

A model of the proposed structures, which are formed depending on the molecule used as precursor, are plotted in Fig. 5.

This connectivity was also corroborated by the XPS spectra. Fig. 6 shows XPS detailed peaks for G100 and T100 (as E100 did not present detectable C content, XPS is not included for C1s). There are two important features in C1s peak (Fig. 6a) for the hybrid films: the increase of intensity, caused by a higher C content in T100 already mentioned, and the shift of the peak to lower binding energies (BE) in T100, which means a higher ratio of C—C (~284.6 eV) and C-Si (~284 eV) [23] bonds, related to C—O (~286.4 eV) bonds, which have a higher contribution in G100 spectra [24–26]. The higher C—C content can be justified by the C content of the precursor and the remaining of $-CH_3$ groups characterized by FTIR and the cyclohexyl group.

If Si2p peak is analyzed (Fig. 6b), contribution of Si—C (~100.2–100.4 eV), Si—O—C (~102.1 eV) and Si-O_x (~103.5–104.2 eV) [27,28] bonds needs to be discussed. As expected, the peak of E100 is located at ~104.8 eV due to the chemical state of Si, O/Si ratio of ~2. In contrast, there is a shift to lower BE in the case of G100 (~102.6 eV) and it is more pronounced in T100 (~101.8 eV). This fact shows that GPTMS has lower relative concentration of Si—C bonds than T100 and a higher ratio of Si—O—C bonds, which is consistent with the FTIR data and the proposed structures.

One common issue for all the hybrid films was the smooth surface obtained, Fig. 7 shows AFM images of the films deposited using a plasma power of 100 W. The surfaces roughness for films deposited from ETHER, GPTMS and TRIMO were 0.406, 0.435 and 2.115 nm, respectively. This fact makes evident that a higher C content, i.e. organic character, in the hybrid films results in higher roughness.

3.1.3. Tuning connectivity of organosilica films by modifying plasma power

Another important factor, which tunes connectivity, is the plasma power. It is important to point out that a minimum plasma power of 80 W is needed to achieve a film when ETHER is used as precursor and still the deposition rate of this process is too low (< 1 nm/cycle). The incorporation of epoxide groups to the precursor molecule decreases the plasma power needed to grow the film, down to 60 W, because of the higher reactivity of the mentioned epoxide groups, particularly in

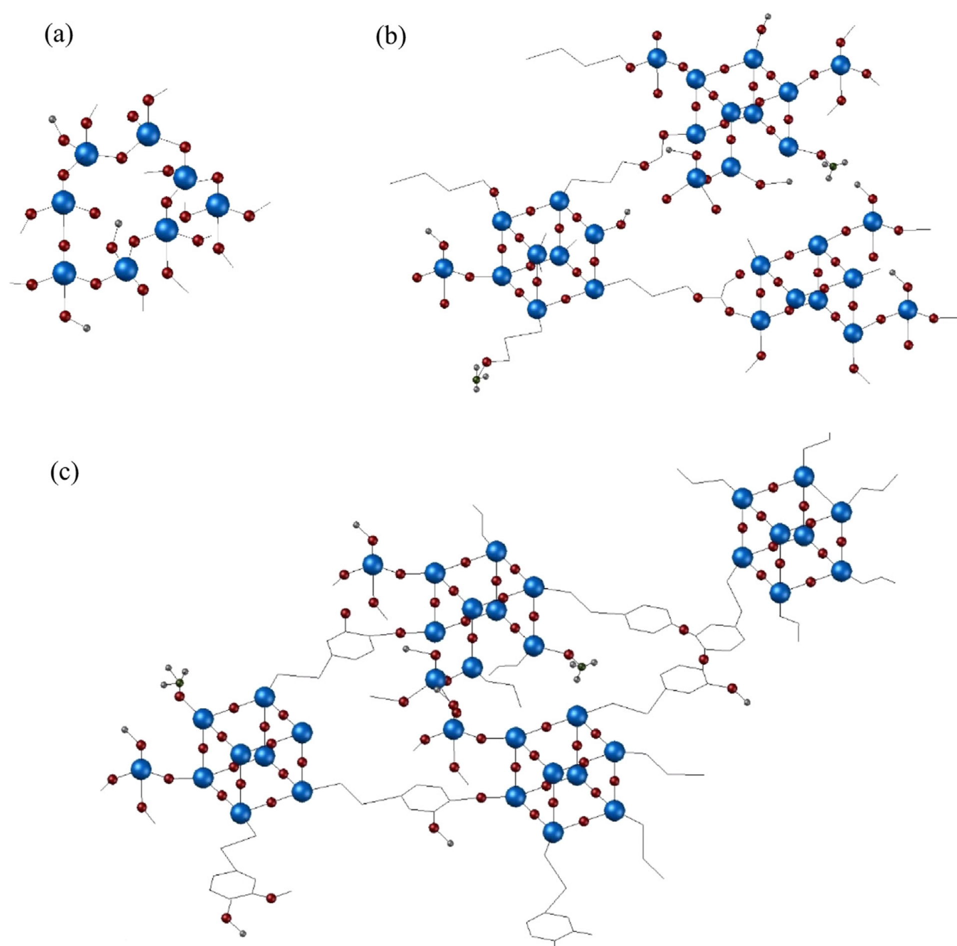

Fig. 5. Structure of organosilica films using (a) ETHER, (b) GPTMS and (c) TRIMOS as precursors.

TRIMO, but adhesion to the substrate is not good enough [29]. In order to elucidate the influence of power in the growth of the films, Fig. 8 shows deposition rates and thickness of the films depending on the precursor and plasma power. Above the minimum plasma power needed, the deposition rate of all the deposited films was higher than 3.5 nm/cycle. In E-films, the deposition rate is too low for plasma powers below 120 W because of the lower reactivity of the molecule. In G-films, the deposition rate slightly diminishes with plasma power, due to the fact the fragmentation of the organic molecule, with the consequent diminution in C content, as it has been explained. In contrast, the augment of plasma power increases the efficiency of molecules incorporated into the film, although the C content also diminishes

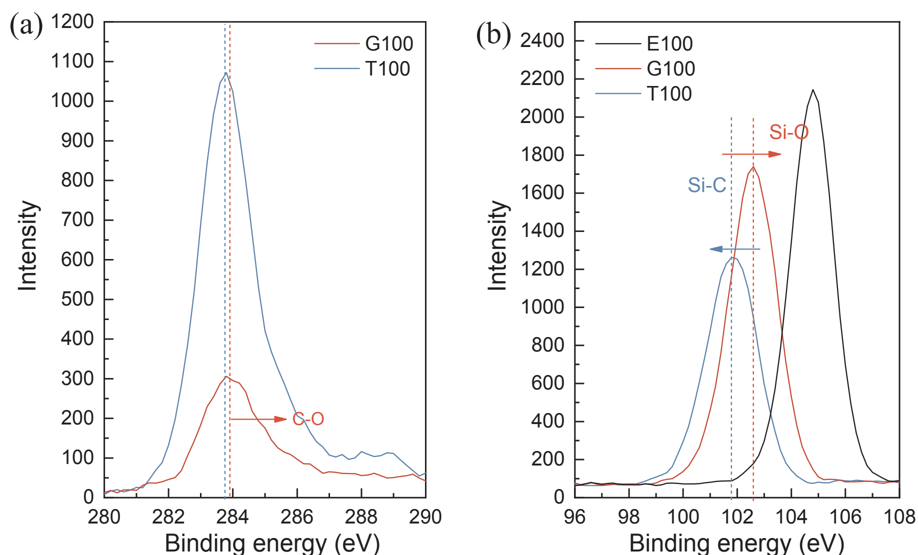

Fig. 6. XPS detailed peaks of hybrid films deposited at 100 W: (a) C1s and (b) Si2p.

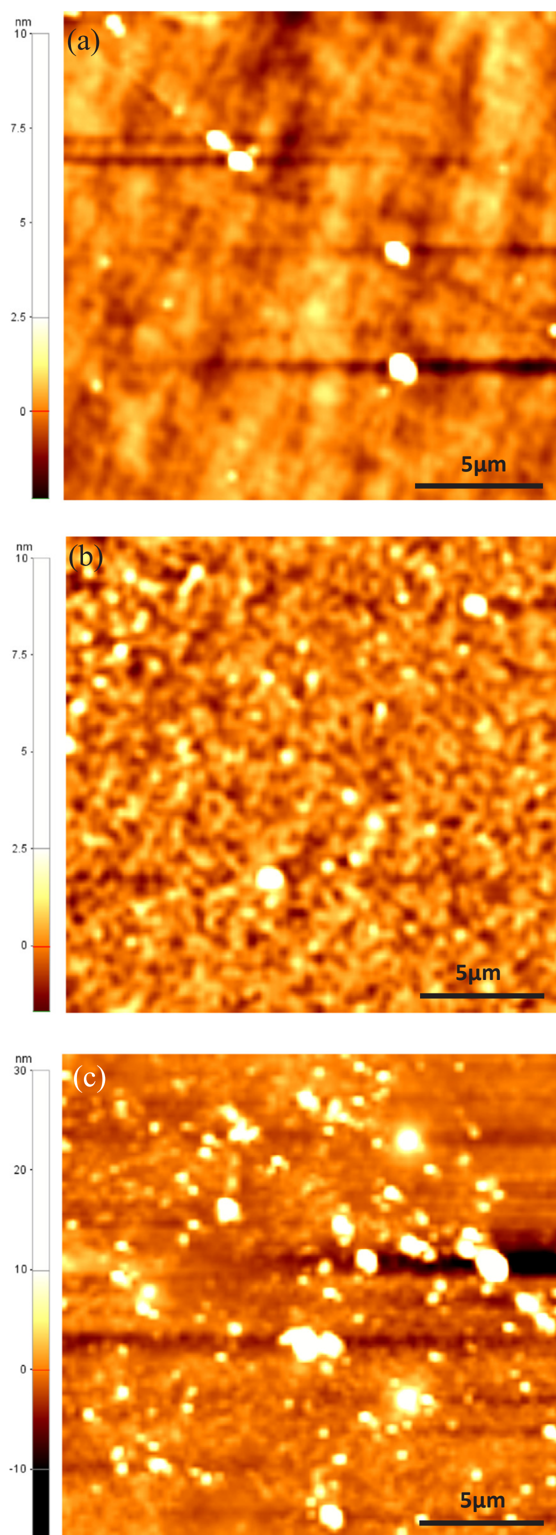

Fig. 7. AFM images of hybrid films deposited at 100 W using: (a) ETHER, (b) GPTMS and (c) TRIMO as precursors.

because of the loss of $-CH_3$ or $-CH_2$ groups, which will be discussed later.

Additionally, as it has been previously mentioned, tuning the plasma power can change C content and connectivity of the films. Fig. 9 shows FTIR spectra of the deposited coatings for each of the precursors used depending on the plasma power. From the obtained results, it was confirmed in all the cases that when higher plasma power is used during deposition, an increase in the intensity of the peak located at ~1075 cm^{-1} occurs, which is an indicator of the formation of new Si—O—Si bonds [19]. In addition, the formation of symmetrical cages diminishes, associated to a decrease of the intensity of the peak located at 1040 cm^{-1}. Another issue to point out is the shift of Si—O—Si associated peak to higher wavenumbers approaching to a value of 1065 cm^{-1}, which corresponds to SiO_2-like structure [16,17] in the case of E-films (Fig. 9a) and additional opening of cages in the cases of G- (Fig. 9b) and T-films (Fig. 9c) [15]. As well as in the cases already explained, peaks suggesting the presence of unreacted epoxy rings were not observed, so a connected network was formed.

As it has been explained, the use of TRIMO as precursor leads to films with higher $-CH_3$ groups in the network, but the concentration of $Si-CH_3$ (1260 cm^{-1}) [16] is reduced when plasma power increases (Fig. 9c) and it is negligible for films deposited at 120 W leading to a higher ratio of Si—O—Si bonds.

If the XPS detailed spectra are analyzed (Fig. 10), additional issues can be pointed out. As it has been mentioned above, the increase in plasma power causes a diminution in organic character of the films. Consequently, the peaks associated to C1s and Si2p should shift to higher BE due to the chemical state of the species [27,28]. Nevertheless, a shift to lower BE values of C1s peaks was observed in XPS spectra with the increase of power. This phenomenon can be attributed to C vacancy-like defects in the structure [30] induce by the higher energy of the process and the disappearance of $-CH_3$ groups [31]. The Si2p peak in all the cases experienced a shift to higher BE increasing plasma power due to the higher SiO_x ratio already reported.

3.2. Stiffness of hybrid films

Mechanical properties of hybrid films are strongly conditioned by their chemical composition and connectivity [4]. To elucidate how chemical composition and connectivity affects mechanical properties, Fig. 11 shows the elastic modulus of the deposited films. Films deposited using ETHER as precursor showed the higher elastic modulus values because of the higher SiO_2-like structure ratio, i.e. the inorganic character. On the other hand, films deposited from TRIMO, showed lower stiffness due to the remaining CH_3 groups as well as the higher fraction of organic network previously characterized [32]. Despite of their considerable higher organic character, the elastic modulus of T-films is in the same range of E-films due to their high concentration of symmetric cages that leads to a more compact structure and, consequently, to a high elastic modulus, near one order of magnitude higher than previously published coatings deposited by sol-gel method as a result of the more energetic process [6]. Those values are in the order of films deposited using plasma-enhanced chemical deposition (PECVD) reported by H. Li et al. [33]. Additionally, compared with E- and G-films, the use of TRIMO as precursor promotes cross-linking, more preservation of the backbone and Si—C bonds [34].

Although the composition of E-films is similar independently on the plasma power, the increase of plasma power in their deposition causes augment of the elastic modulus, which can be due to the higher concentration of Si—O—Si bonds and a diminution in the cages fraction, i.e. change in connectivity of the film. The same tendency is observed in T-films, but in this case, the enhancement in the elastic modulus is not only caused by the change in connectivity but also by the chemical composition, as the inorganic character of the film is higher when using higher plasma powers. However, G-films behaves differently, there is a diminution in the elastic modulus, this fact is attributed to the C vacancy-like defects discussed in the previous section, which causes the detriment of mechanical properties of the films.

3.3. Fluorinated organosilica films

In order to achieve higher hydrophobicity in coatings [35,36], FDTS was successfully incorporated in coatings with high C contents

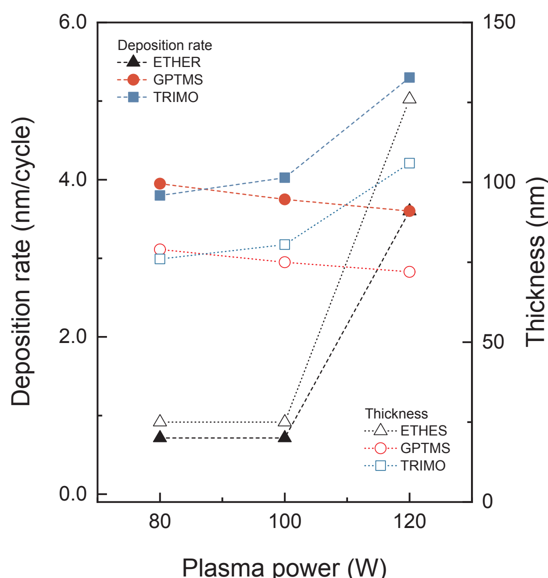

Fig. 8. Deposition rate and thickness of hybrid films as function of precursor and plasma power.

deposited at 100 W, i.e. G100 and T100. The incorporation of the molecules was successfully achieved by atmospheric plasma deposition and the contents in both cases was around 15 at%. In order to analyze the influence in the chemical composition of the hybrid films, Fig. 12 shows atomic contents (Fig. 12a) and ratios (Fig. 12b) of non-fluorinated and fluorinated hybrid films. The amount of Si and O atoms follows the same tendency in both cases, as expected an increase of Si at.% and reduction of O at.% were induced. The relative carbon content in G/F increases when fluorinated molecules are incorporated into the film due to the C atoms of FDTS. Conversely, it diminishes in T/F, fact that can be due to the loss of $-CH_3$ groups caused by the bonding reaction of FDTS with TRIMO molecules.

The incorporation of fluorinated chains in the structure of the hybrid films also causes changes in connectivity. These changes were monitored by FTIR and results are shown in Fig. 13. In the FTIR spectrum of G/F (Fig. 13a), new bands corresponding to C−F vibration appears at 1150–1250 cm^{-1} [37] and the peak associated to Si−O−Si remains mainly the same, indicating that there is no significant change in Si−O−Si connectivity and fluorinated chains are incorporated in open cages. In the case of T/F (Fig. 13b), there is an appreciable change in connectivity caused by the loss of $-CH_3$ mentioned above (Fig. 13c), formation of Si−O−Si networks is promoted in detriment of cages, leading to a more random structure.

Additionally, the efficiency of the atmospheric plasma deposition strongly diminishes, more than one order of magnitude. This fact is attributed to the preferential orientation of fluorinated molecules due to the low surface energy of FDTS that causes migration of fluorinated tails to the film-air interface during the film growth [38,39]. Consequently, the enrichment of the surface in F atoms reduces surface energy inhibiting the deposition of the precursor and, therefore, the efficiency of the process.

In order to study the increase of the hydrophobicity of the films due to the incorporation of the fluorinated molecules, water contact angle measurements were carried out. Fig. 14 shows the values of the water contact angles and images for the G- and T-based films. The fluorinated films caused an augment in water contact angle of 23.4 and 21.0% in G- and T-based films, respectively, increasing hydrophobicity of the surfaces. This fact supports the efficiency of the atmospheric plasma deposition for the deposition fluorinated organosilica films.

4. Conclusions

Atmospheric plasma deposition was successfully used to deposited organosilica hybrid films and fluorinated organosilica hybrid films. The strong influence of epoxy groups in the precursor molecule as a consequence of changes in activity and fragmentation in the connected organic networks was discussed. Chemical composition and connectivity of hybrid films could be tuned and controlled by the use of different precursors and plasma power during deposition. Results confirmed that the incorporation of epoxide groups in the precursor molecules favors formation of cages in the structure. The use of precursors with more C atoms in the molecule considerably increases the organic character of the films and the incorporation of cyclohexyl groups increases stability of the compound and leads to a higher concentration of $-CH_3$ group in films. The increase in power induce shifting to a more inorganic network and diminishes concentration of $-CH_3$. These facts make possible tuning of mechanical properties as it is strongly dependent on chemical composition and connectivity.

Incorporation of fluorinated molecules into the hybrid network was also successfully achieved by atmospheric plasma deposition with the consequent increase of hydrophobicity. Apparently, these molecules were bonded to open cages in the case of GPTMS and replacing $-CH_3$ in TRIMO based films changing composition and connectivity of hybrid films. Due to the preferential orientation of the chains caused by the

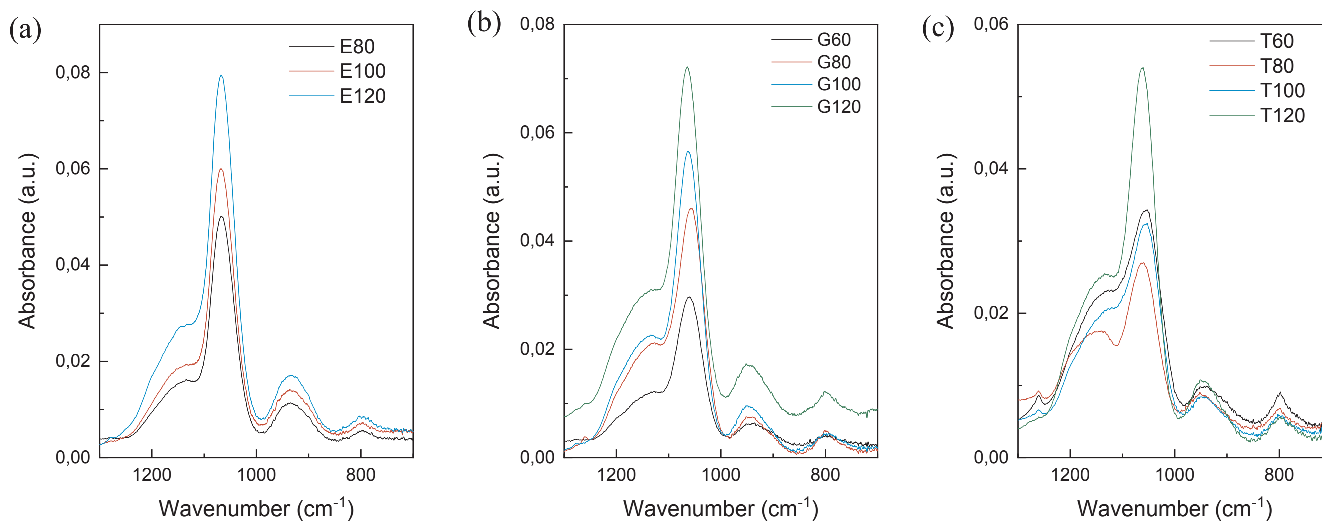

Fig. 9. FTIR spectra of deposited hybrid films using (a) ETHER, (b) GPTMS and (c) TRIMO as precursors.

Fig. 10. Detailed XPS spectra: C1s (a,b) and Si2p (c-e) of deposited hybrid films using (c) ETHER, (a,d) GPTMS and (b,e) TRIMO as precursors.

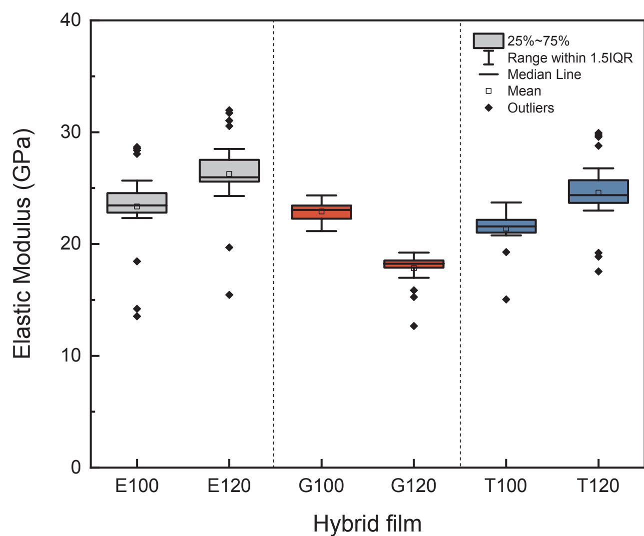

Fig. 11. Elastic modulus of deposited hybrid films.

low surface energy, which increases F concentration in surface, efficiency of the deposition process was significantly inhibited.

CRediT authorship contribution statement

R. Moriche: Conceptualization, Methodology, Investigation, Writing - original draft, Writing - review & editing. **Y. Ding:** Conceptualization, Methodology, Investigation, Writing - review & editing. **S. Dong:** Conceptualization, Methodology. **O. Zhao:** Investigation, Writing - review & editing. **R.H. Dauskardt:** Project administration, Funding acquisition, Supervision, Conceptualization, Methodology, Writing - review & editing.

Declaration of Competing Interest

The authors declare that they have no known competing financial interests or personal relationships that could have appeared to influence the work reported in this paper.

Acknowledgements

This work was supported by the Durable Modules Consortium (DuraMAT), an Energy Materials Network Consortium funded by the

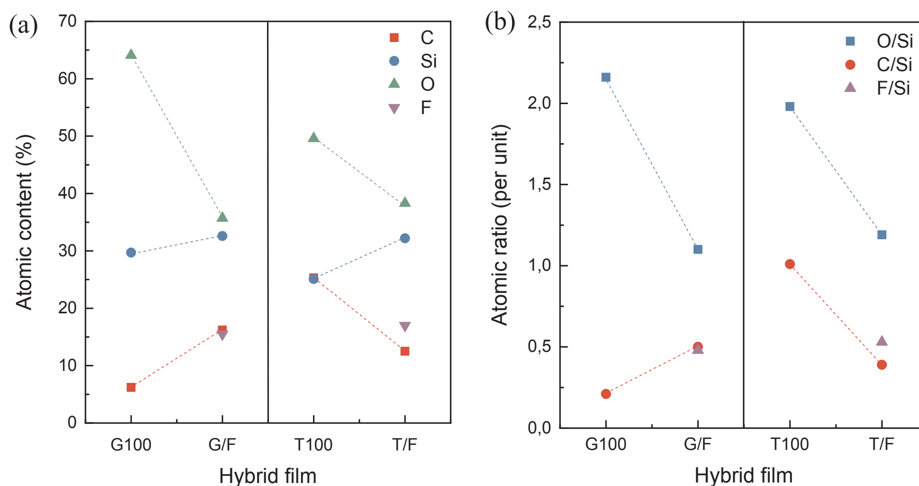

Fig. 12. Chemical composition of non-fluorinated (G100 and T100) and fluorinated (G/F and T/F) deposited at 100 W: (a) Si, O and C atomic contents; and (b) O/Si, C/Si and F/Si atomic ratios.

U.S. Department of Energy, Office of Energy Efficiency and Renewable Energy, Solar Energy Technologies Office. The authors acknowledge funding from Ministerio de Educación, Cultura y Deporte of Spain and Fulbright Commission for José Castillejo and Fulbright Programs grants.

Part of this work was performed at the Stanford Nano Shared Facilities (SNSF) and the Stanford Nanofabrication Facility (SNF).

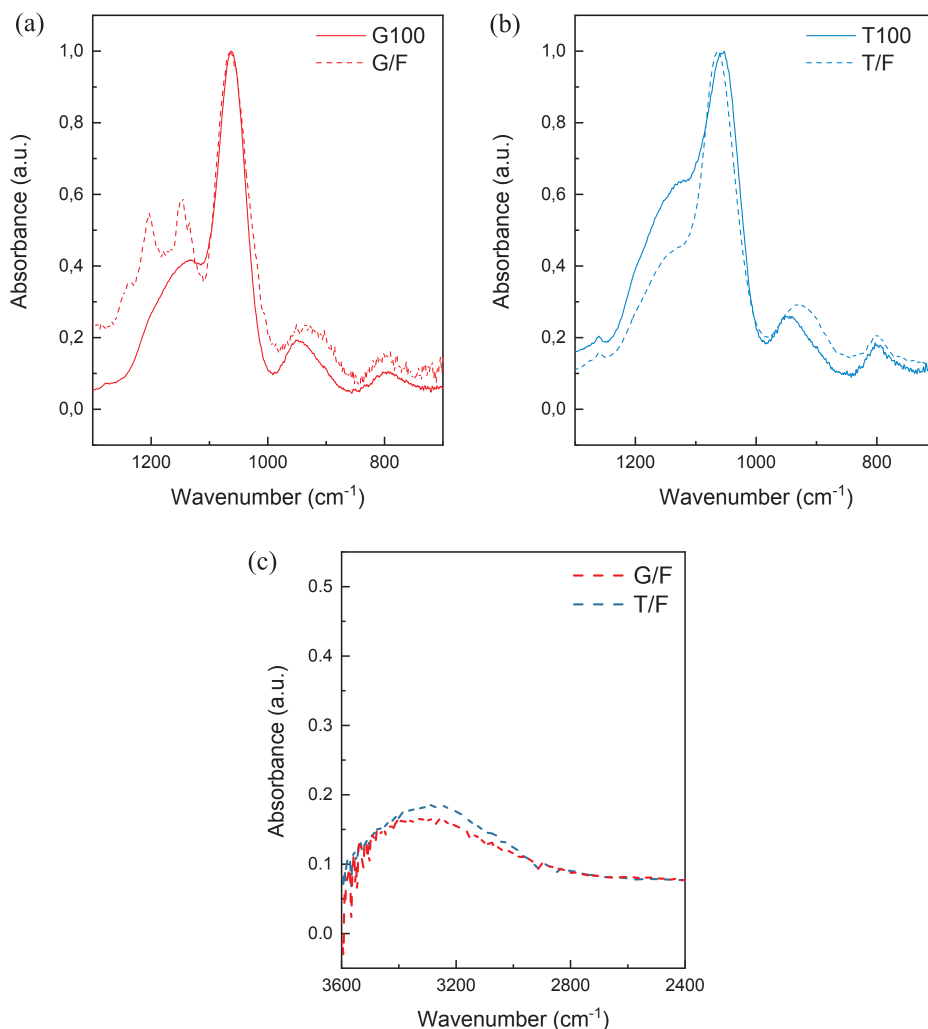

Fig. 13. FTIR spectra of non-fluorinated (G100 and T100) and fluorinated (G/F and T/F) films deposited at 100 W using (a, c) GPTMS and (b, c) TRIMO as precursors: (a, b) 700–1300 cm^{-1} and (b) 2400–3600 cm^{-1}.

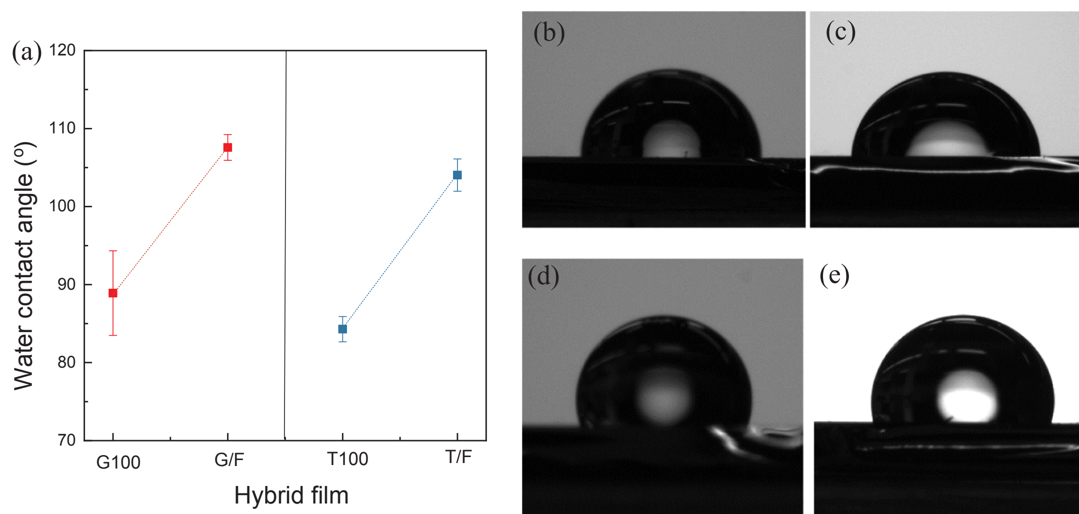

Fig. 14. Influence of the fluorinated molecules in hydrophobicity of films deposited at 100 W: (a) water contact angle of non-fluorinated (G100 and T100) and fluorinated (G/F and T/F) and optical images of water drops on (b) G100, (c) G/F, (d) T100 and (e) T/F films.

References

[1] L. Xu, Y. Shen, L. Wang, Y. Ding, Z. Cai, Preparation of vinyl silica-based organic/inorganic nanocomposites and superhydrophobic polyester surfaces from it, Colloid Polym. Sci. 293 (2015) 2359–2371, https://doi.org/10.1007/s00396-015-3624-6.

[2] F. Mammeri, E. Le Bourhis, L. Rozes, C. Sanchez, Mechanical properties of hybrid organic-inorganic materials, J. Mater. Chem. 15 (2005) 3787–3811, https://doi.org/10.1039/b507309j.

[3] O.H. Teresa, C.K. Choi, Comparison between SiOC thin film by plasma enhance chemical vapor deposition and SiO2 thin film by Fourier transform infrared spectroscopy, J. Korean Phys. Soc. 56 (2010) 1150–1155, https://doi.org/10.3938/jkps.56.1150.

[4] S. Dong, J. Han, Z. Zhao, R.H. Dauskardt, Role of carbon bridge length of organosilicate precursors on the atmospheric plasma deposition of transparent bilayer protective coatings on plastics, Plasma Process. Polym. 13 (2016) 1051–1058, https://doi.org/10.1002/ppap.201600024.

[5] Y. Ding, Q. Xiao, R.H. Dauskardt, Molecular design of confined organic network hybrids with controlled deformation rate sensitivity and moisture resistance, Acta Mater. 142 (2018) 162–171, https://doi.org/10.1016/j.actamat.2017.09.060.

[6] Y. Ding, S. Dong, J. Han, D. He, Z. Zhao, R.H. Dauskardt, Optically transparent protective coating for plastics using dual spray and atmospheric plasma deposition, Adv. Mater. Interfaces 5 (2018) 1–9, https://doi.org/10.1002/admi.201701433.

[7] J. Yang, Y. Pu, D. Miao, X. Ning, Fabrication of durably superhydrophobic cotton fabrics by atmospheric pressure plasma treatment with a siloxane precursor, Polymers (Basel) 10 (2018) 460, https://doi.org/10.3390/polym10040460.

[8] L. Matějka, O. Dukh, J. Brus, W.J. Simonsick, B. Meissner, Cage-like structure formation during sol-gel polymerization of glycidyloxypropyltrimethoxysilane, J. Non Cryst. Solids 270 (2000) 34–47, https://doi.org/10.1016/S0022-3093(00)00074-0.

[9] A. Vogelsang, A. Ohl, R. Foest, K. Schröder, K.D. Weltmann, Hydrophobic coatings deposited with an atmospheric pressure microplasma jet, J. Phys. D. Appl. Phys. 43 (2010), https://doi.org/10.1088/0022-3727/43/48/485201.

[10] A. El-Shafei, H. Helmy, A. Ramamoorthy, P. Hauser, Nanolayer atmospheric pressure plasma graft polymerization of durable repellent finishes on cotton, J. Coatings Technol. Res. 12 (2015) 681–691, https://doi.org/10.1007/s11998-015-9665-4.

[11] D. Merche, N. Vandencasteele, F. Reniers, Atmospheric plasmas for thin film deposition: A critical review, Thin Solid Films 520 (2012) 4219–4236, https://doi.org/10.1016/j.tsf.2012.01.026.

[12] R. Molina, J.M. Teixidó, C.W. Kan, P. Jovančić, Hydrophobic coatings on cotton obtained by in situ plasma polymerization of a fluorinated monomer in ethanol solutions, ACS Appl. Mater. Interfaces 9 (2017) 5513–5521, https://doi.org/10.1021/acsami.6b15812.

[13] W.C. Oliver, G.M. Pharr, Measurement of hardness and elastic modulus by instrumented indentation: Advances in understanding and refinements to methodology, J. Mater. Res. 19 (2004) 3–20, https://doi.org/10.1557/jmr.2004.19.1.3.

[14] S. Dong, Z. Zhao, R.H. Dauskardt, Dual precursor atmospheric plasma deposition of transparent bilayer protective coatings on plastics, ACS Appl. Mater. Interfaces 7 (2015) 17929–17934, https://doi.org/10.1021/acsami.5b04622.

[15] L. Cui, A.N. Ranade, M.A. Matos, L.S. Pingree, T.J. Frot, G. Dubois, R.H. Dauskardt, Atmospheric plasma deposited dense silica coatings on plastics, ACS Appl. Mater. Interfaces 4 (2012) 6587–6598, https://doi.org/10.1021/am301723d.

[16] L. Zhang, R. Ljazouli, P. Lefaucheux, T. Tillocher, R. Dussart, Y.A. Mankelevich, J.-F. de Marneffe, S. de Gendt, M.R. Baklanov, Low damage cryogenic etching of porous organosilicate low-k materials using SF6/O2/SiF4, ECS J. Solid State Sci. Technol. 2 (2013) N131–N139, https://doi.org/10.1149/2.001306jss.

[17] M.R. Baklanov, J.-F. de Marneffe, D. Shamiryan, A.M. Urbanowicz, H. Shi, T.V. Rakhimova, H. Huang, P.S. Ho, Plasma processing of low-k dielectrics, 041101, J. Appl. Phys. 113 (2013), https://doi.org/10.1063/1.4765297.

[18] J. Brus, M. Špírková, D. Hlavatá, A. Strachota, Self-organization, structure, dynamic properties, and surface morphology of silica/epoxy films as seen by solid-state NMR, SAXS, and AFM, Macromolecules 37 (2004) 1346–1357, https://doi.org/10.1021/ma035608h.

[19] S. Liu, H. Zhou, H. Wang, Y. Zhao, H. Shao, Z. Xu, Z. Feng, D. Liu, T. Lin, Argon plasma treatment of fluorine-free silane coatings: a facile, environment-friendly method to prepare durable, superhydrophobic fabrics, Adv. Mater. Interfaces 4 (2017), https://doi.org/10.1002/admi.201700027.

[20] A.N. Khramov, V.N. Balbyshev, N.N. Voevodin, M.S. Donley, Nanostructured sol-gel derived conversion coatings based on epoxy- and amino-silanes, Prog. Org. Coatings 47 (2003) 207–213, https://doi.org/10.1016/S0300-9440(03)00140-1.

[21] J.M. Antonucci, S.H. Dickens, B.O. Fowler, H.H.K. Xu, Chemistry of silanes: Interfaces in dental polymers and composites, J. Res. Natl. Inst. Stand. Technol. 110 (2005) 541, https://doi.org/10.6028/jres.110.081.

[22] R.N. Jana, H. Bhunia, Thermal stability and proton conductivity of silane based nanostructured composite membranes, Solid State Ionics 178 (2008) 1872–1878, https://doi.org/10.1016/j.ssi.2007.11.036.

[23] X. Sun, F. Zhang, Y. Chen, Z. Cheng, Y. Su, J. Hang, L. Jin, N. Li, D. Shang, L. Shi, Preparation and properties of crosslinked network coatings based on perfluoropolyether/poly(dimethyl siloxane)/acrylic polyols for marine fouling-release applications, J. Appl. Polym. Sci. 132 (2015), https://doi.org/10.1002/app.41860.

[24] A. Walkiewicz-Pietrzykowska, J. Cotrino, A.R. González-Elipe, Deposition of thin films of SiOxCyH in a surfatron microwave plasma reactor with hexamethyldisiloxane as precursor, Chem. Vap. Depos. 11 (2005) 317–323, https://doi.org/10.1002/cvde.200506374.

[25] N. Satyanarayana, N.N. Gosvami, S.K. Sinha, M.P. Srinivasan, Friction, adhesion and wear durability of an ultra-thin perfluoropolyether-coated 3-glycidoxypropyltrimethoxy silane self-assembled monolayer on a Si surface, Philos. Mag. 87 (2007) 3209–3227, https://doi.org/10.1080/14786430701261455.

[26] Z.H. Mo, Z. Luo, Q. Huang, J.P. Deng, Y.X. Wu, Superhydrophobic hybrid membranes by grafting arc-like macromolecular bridges on graphene sheets: Synthesis, characterization and properties, Appl. Surf. Sci. 440 (2018) 359–368, https://doi.org/10.1016/j.apsusc.2017.12.268.

[27] Y.L. Khung, S.H. Ngalim, A. Scaccabarozzi, D. Narducci, Formation of stable Si-O-C submonolayers on hydrogenterminated silicon(111) under low-temperature conditions, Beilstein J. Nanotechnol. 6 (2015) 19–26, https://doi.org/10.3762/bjnano.6.3.

[28] K.D. Esmeryan, E.I. Radeva, I.D. Avramov, Durable superhydrophobic carbon soot coatings for sensor applications, J. Phys. D. Appl. Phys. 49 (2015), https://doi.org/10.1088/0022-3727/49/2/025309.

[29] C. Croutxé-barghorn, A. Chemtob, D. Versace, C. Belon, Photopolymerizable Hybrid Sol-gel : New Opportunities for UV-cured Coatings, 19 (n.d.).

[30] K. Ganesan, S. Ghosh, N. Gopala Krishna, S. Ilango, M. Kamruddin, A.K. Tyagi, A comparative study on defect estimation using XPS and Raman spectroscopy in few layer nanographitic structures, Phys. Chem. Chem. Phys. 18 (2016) 22160–22167, https://doi.org/10.1039/c6cp02033j.

[31] K. Mudiyanselage, M. Trenary, Adsorption and thermal decomposition of acetaldehyde on Si(111)-7 × 7, Surf. Sci. 603 (2009) 3215–3221, https://doi.org/10.1016/j.susc.2009.09.005.

[32] R. Nenashev, Y. Wang, C. Liu, N. Kotova, K. Vorotilov, J. Zhang, S. Wei, D. Seregin, A. Vishnevskiy, J. (Jim) Leu, M.R. Baklanov, Effect of Bridging and Terminal Alkyl Groups on Structural and Mechanical Properties of Porous Organosilicate Films, ECS J. Solid State Sci. Technol. 6 (2017) N182–N188. doi:10.1149/2.0071710jss.

[33] H. Li, Y. Lin, T.Y. Tsui, J.J. Vlassak, The effect of porogen loading on the stiffness and fracture energy of brittle organosilicates, J. Mater. Res. 24 (2009) 107–116, https://doi.org/10.1557/jmr.2009.0005.

[34] Y. Lin, Y. Xiang, T.Y. Tsui, J.J. Vlassak, PECVD low-permittivity organosilicate glass coatings: Adhesion, fracture and mechanical properties, Acta Mater. 56 (2008) 4932–4943, https://doi.org/10.1016/j.actamat.2008.06.007.

[35] M.I. Kayes, A.J. Galante, N.A. Stella, S. Haghanifar, R.M.Q. Shanks, P.W. Leu, Stable lotus leaf-inspired hierarchical, fluorinated polypropylene surfaces for reduced bacterial adhesion, React. Funct. Polym. 128 (2018) 40–46, https://doi.org/10.1016/j.reactfunctpolym.2018.04.013.

[36] P. Wu, S. Zhang, H. Yang, Y. Zhu, J. Chen, Preparation of emulsion-templated fluorinated polymers and their application in oil/water separation, J. Polym. Sci. Part A Polym. Chem. (2018) 1508–1515, https://doi.org/10.1002/pola.29030.

[37] B. Lebeau, C. Marichal, A. Mirjol, G.J.D.A.A. Soler-Illia, R. Buestrich, M. Popall, L. Mazerolles, C. Sanchez, Synthesis of highly ordered mesoporous hybrid silica from aromatic fluorinated organosilane precursors, New J. Chem. 27 (2003) 166–171, https://doi.org/10.1039/b206924p.

[38] M. Ochi, N. Ichikawa, R. Shiota, Y. Hattori, M. Harada, M. Hara, H. Uchida, Surface properties of alicyclic epoxy coatings modified with reactive copolymer containing fluorinated side chains, J. Coatings Technol. Res. 11 (2014) 913–921, https://doi.org/10.1007/s11998-014-9604-9.

[39] Y. Guo, D. Tang, F. Yang, Transparent fluorinate acrylic polyurethane with hydrophobicity obtained by crosslinking of hydroxyl-containing fluoroacrylate copolymer with HDI trimer, Mater. Sci. Pol. 33 (2015) 451–459, https://doi.org/10.1515/msp-2015-0076.